Phase diagrams for surface alloys

A. Christensen, A. V. Ruban, P. Stoltze, K. W. Jacobsen, H. L. Skriver, and J. K. Nørskov
Center for Atomic-scale Materials Physics (CAMP), Department of Physics, Technical University of Denmark, DK-2800 Lyngby, Denmark

F. Besenbacher
Center for Atomic-scale Materials Physics (CAMP), Institute of Physics and Astronomy, University of Aarhus, DK 8000 Aarhus, Denmark

(Received 22 November 1996)

We discuss surface alloy phases and their stability based on surface phase diagrams constructed from the surface energy as a function of the surface composition. We show that in the simplest cases of pseudomorphic overlayers there are four generic classes of systems, characterized by the sign of the heat of segregation from the bulk and the sign of the excess interactions between the atoms in the surface (the surface mixing energy). We also consider the more complicated cases with ordered surface phases, nonpseudomorphic overlayers, second layer segregation, and multilayers. The discussion is based on density-functional calculations using the coherent-potential approximation and on effective-medium theory. We give self-consistent density-functional results for the segregation energy and surface mixing energy for all combinations of the transition and noble metals. Finally we discuss in detail the cases Ag/Cu(100), Pt/Cu(111), Ag/Pt(111), Co/Cu(111), Fe/Cu(111), and Pd/Cu(110) in connection with available experimental results. [S0163-1829(97)07534-6]

I. INTRODUCTION

When one metal is deposited on another, one observes a number of different phenomena. The deposited metal may form islands on the substrate or it may alloy into the first or deeper layers.[1–7] Alloying may take place both in cases where the two metals form an alloy in the bulk[8–17] and in cases where they do not.[16,18–26,28] Also, one observes new overlayer phases with a structure and periodicity substantially different from that of the substrate. Furthermore, the mismatch between the overlayer and the substrate may be so large that misfit dislocation structures are formed even after a single layer has been deposited.[27,29,30] In some cases the structures that are formed during deposition reflect the thermodynamic ground state of the system, but often the structures are metastable, and the observations partly reflect the kinetics of the deposition, diffusion, and growth processes.

The wealth of phenomena that has been reported makes it important to be able to categorize the observed behavior in some way, and the recent literature shows many efforts in the direction of developing the thermodynamics of surface alloy formation.[31–35] In this endeavor it is important to note that at ordinary temperatures the entropy driven diffusion of the deposited material into the bulk is usually slow. Hence, at time scales which are long in terms of kinetics but short in terms of bulk diffusion, a local equilibrium may be established in the surface region.[35] As a result, surface structures formed by depositing elements on surfaces are very stable in particular temperature ranges and one may therefore consider equilibrium not in the infinitely large system but in a local region near the surface with a finite concentration of the deposited element.

With this quasiequilibrium in mind we concentrate in the present paper on the thermodynamics of surface alloy formation. In particular, we suggest a transparent way of understanding the phase diagram of a surface alloy, in analogy with phase equilibria in the bulk. We construct a surface phase diagram, and introduce a number of generic classes of systems with similar behavior. We support the analysis by calculations of the detailed energetics of a few systems chosen to illustrate the different classes. The system-specific results presented are based on self-consistent, density-functional (DFT) calculations and the more approximate effective-medium theory. We do not consider small islands of one metal on another or the kinetics by which these islands are formed or agglomerated during the approach to equilibrium. Our analysis therefore applies only to flat surfaces or at least large islands where edge effects may be neglected.

We start by a very general discussion of the energetics of metal on metal systems and introduce the concepts used later in the paper. For each of the cases we consider, we discuss the calculation of the phase diagram in the light of the experimental results for the system. Finally, we present a complete database constructed from the self-consistent density-functional calculations of the segregation energies and the surface mixing energies for all combinations of the transition metals. This database may serve as a first entry into the energetics of surface alloys.

II. THE ENERGETICS OF A SURFACE ALLOY

We first define the surface energy in rather general terms. Consider an alloy consisting of N^A atoms of type A and N^B atoms of type B, the total number of atoms being $N=N^A+N^B$. Of these N atoms N_s are residing at the surface, while the remaining $N_b=N-N_s$ are bulk atoms. We assume, for simplicity, that all surface and bulk atoms of a given kind (A or B) are equivalent. The description can easily be generalized if this is not the case. The composition of

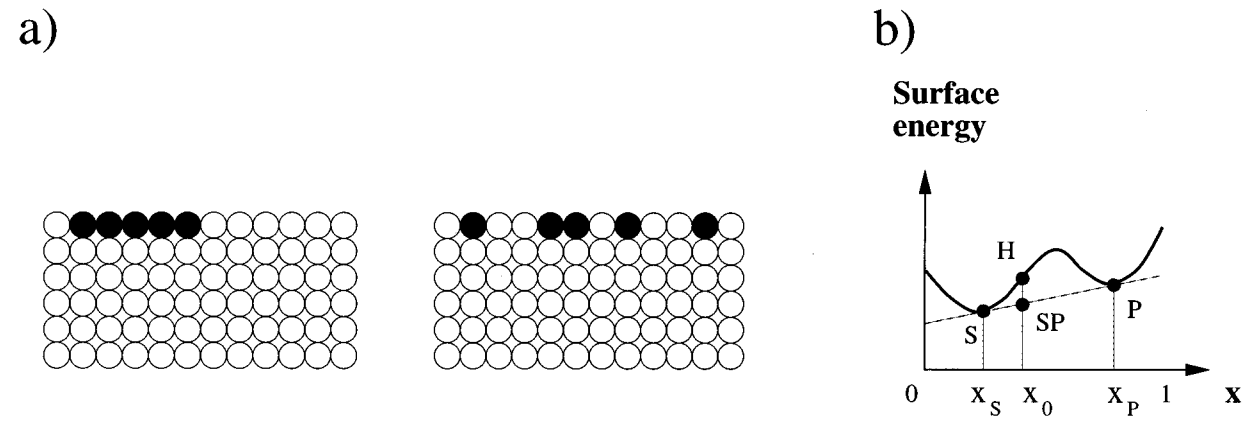

FIG. 1. (a) Sketch of a pure pseudomorphic overlayer phase and a pseudomorphic surface alloy phase. (b) Sketch of surface energy versus coverage x of deposited material. We have also illustrated the common tangent principle in this figure. See text for details.

the surface may differ from the bulk. We denote by N_s^A the number of A atoms in the surface with a similar convention for the number of B atoms. We refer to the surface, bulk, and average concentration of B atoms as x_s, x_b, and x, respectively, and we only consider the case, where a single layer in the surface has a composition different from that of the bulk. The formulas below are easily generalized to the case, where several layers deviate from the bulk composition.

We have collected the notation with the relations between the variables below:

$$N=N^A+N^B=N_s+N_bN^{A,B}=N_s^{A,B}+N_b^{A,B}Nx=N_sx_s+N_bx_b,$$

$$x_s=\frac{N_s^B}{N_s},\quad x_b=\frac{N_b^B}{N_b},\quad x=\frac{N^B}{N}. \tag{1}$$

We write the total energy of the alloy system (in the limit $N\to\infty$) as

$$E(N_s^A,N_s^B;N_b^A,N_b^B)=N_se_s(x_s,x)+N\epsilon_b(x). \tag{2}$$

In the following, upper and lower case letters refer to extensive and intensive (per atom) quantities, respectively. The bulk state is the reference state, which may be a dilute solution, an ordered, or a random alloy. The bulk state has an average energy $\epsilon_b(x)$ per atom. Since we work with a fixed number of A and B atoms, only two variables in Eq. (2) are independent. The first term, e_s, on the right-hand side of Eq. (2) is the surface energy per surface atom as can easily be seen by calculating the energy with and without a surface present:

$$e_s=\frac{1}{N_s}[E(N_s^A,N_s^B;N^A-N_s^A,N^B-N_s^B)-E(0,0;N^A,N^B)]. \tag{3}$$

We will also consider the energy of surface segregation for a B atom. We define this as the energy of interchanging a B atom in the bulk with an A atom atom in the surface:

$$e_{\text{segr}}=E(N_s^A-1,N_s^B+1;N_b^A+1,N_b^B-1)-E(N_s^A,N_s^B;N_b^A,N_b^B), \tag{4}$$

$$=N_s\left[e_s\left(x_s+\frac{1}{N_s},x\right)-e_s(x_s,x)\right]$$

$$=\frac{\partial e_s(x_s,x)}{\partial x_s}. \tag{5}$$

The equilibrium surface concentration (at $T=0$) is found by minimizing the surface energy or equivalently by setting the segregation energy to zero.

A small amount of deposited material on a pure host crystal ($x=0$) is always metastable at nonzero temperatures because there are many more sites in the bulk than in the surface. Hence the gain in entropy by dissolving into the bulk, which is roughly $\Delta S=k\ln(N_b/N_s)$, will drive the deposited material away from the surface. However, close to room temperature bulk diffusion in a metal is usually extremely slow, and a quasiequilibrium may be established in the surface region. It is therefore also of interest to study the partial equilibrium at a surface even when the surface is at a nonequilibrium concentration relative to the bulk. In the following we discuss on the basis of Eq. (3) the quasiequilibrium that occurs, when diffusion between bulk and surface is neglible.

We now concentrate on the surface layer (or perhaps the first few surface layers) and ask the question whether the two components in the surface layer will mix or form separate islands, and if they mix, whether they will mix randomly or form ordered structures. This is completely analogous to the usual treatment of the thermodynamics of two bulk metals. The energetics of the two-dimensional (2D) alloying problem at the surface is determined by the surface energy $e_s(x_s,x)$ as a function of x_s. In general $e_s(x_s,x)$ for a fixed total composition x may look as shown in in Fig. 1(b). We refer to this as a surface energy curve. In Fig. 1(b) we have also illustrated the general common tangent principle.[36,37] Given the surface energy curve $e_s(x)$, the surface alloy with overall concentration x_0 of B atoms may choose either to form a homogeneous solution (H) or to separate into distinct

phases, say (S) and (P) with concentration x_S and x_P, respectively, if the condition $x_S<x_0<x_P$ is fulfilled. Due to overall mass conservation, the relative abundance of (S) and (P) will scale according to the lever rule as x_P-x_0 to x_0-x_S, which also implies that the energy of the phase equilibrium of (S) and (P) will be a straight line between the points (S) and (P) in the surface energy diagram.

Phase separation occurs depending on whether (H) is below or above (SP) in Fig. 1(b). If the surface energy curve $e_s(x)$ is smooth, a general condition for phase separation is that x_S and x_P embrace an interval, where $e^s(x)$ has a negative curvature and that (S) and (P) are points on a common tangent (or an endpoint $x=0$ or $x=1$) touching $e^s(x)$ at the most stable phase combination. If, however, many families of phases compete, e.g., having different underlying structures each with surface energy curves $e_s^{\alpha}(x_s^{\alpha}), e_s^{\beta}(x_s^{\beta}), \ldots$, negative curvature is not a condition for phase separation. We will discuss such cases later.

The above considerations applies to the $T=0$ limit. At finite temperatures one must include entropy effects and the thermodynamic equilibrium is then determined by the overall minimum of the free energy

$$G=E-TS, \tag{6}$$

where S is the entropy. Similar to the 3D bulk alloying case, we may include entropy effects for the surface quasiequilibrium by adding the entropy term of different disordered surface phases. Neglecting differences in the vibrational entropy due to alloying, the main dependence of the entropy on the concentration is the mixing entropy, given by[38]

$$s^{\mathrm{mix}}=-k[x_s^{\alpha}\ln(x_s^{\alpha})+(1-x_s^{\alpha})\ln(1-x_s^{\alpha})], \tag{7}$$

where x_s^{α} is the concentration of the disordered phase α (ordered phases have vanishing mixing entropy).

In analogy with the 3D bulk case, we also define a surface mixing energy by

$$e_s^{\mathrm{mix}}=e_s-e_0-x_s(e_1-e_0), \tag{8}$$

where e_0 and e_1 are the surface energies of the pure substrate and the surface covered with a monolayer of impurities, respectively. The 2D quasiequilibrium is then determined by the minimum of the surface free energy of mixing

$$g^{\mathrm{mix}}=e_s^{\mathrm{mix}}-Ts^{\mathrm{mix}} \tag{9}$$

under the constraint that the average surface impurity concentration is fixed to x_s.

III. CALCULATIONAL DETAILS

We have employed two different computational techniques to obtain surface energies for different binary surface alloy systems. Since we focus on energetic principles rather than the calculations themselves, we only briefly summarize our computational approaches and refer to the literature for more extensive details.

A. CPA calculations

The surface energies were calculated by means of the linear muffin-tin orbitals (LMTO) method in the tight-binding representation using the atomic-sphere approximation (ASA) in conjunction with the coherent-potential approximation (CPA) and a Green's-function technique[39–43] for the semi-infinite surface. The calculations were performed within the local-density approximation for exchange and correlation, using the Perdew-Zunger[44] and Vosko-Wilk-Nusair[45] parametrizations for paramagnetic and spin-polarized calculations, respectively. For the bulk calculations, 240, 285, and 287 k points in the irreducible wedge of the Brillouin zone are used for fcc, bcc, and hcp, respectively. For surface calculations 90, 64, and 90 special k points[46] in the irreducible polygon of the surface Brillouin zone are used for fcc(111), bcc(110), and hcp(0001), respectively. We have included potential and density perturbations in three vacuum layers and nine surface layers, the deeper layers being assumed bulklike. For metallic systems this is sufficient, due to efficient screening. For the Fe/Cu(111) and Co/Cu(111) calculations we have included potential and density perturbations of three vacuum layers and 15 surface layers, because in these cases we consider concentration variations deeper into the bulk.

B. Effective-medium theory (EMT) calculations

The LMTO-ASA method is efficient and accurate when lattice relaxations at the surface or locally around an impurity may be neglected. When relaxation effects and reconstructions become important, we have used the more approximative effective-medium theory (EMT) to calculate the surface energies. As we will show later, surface mixing energies obtained by CPA and EMT are in quite reasonable agreement, indicating that including relaxation effects by means of EMT is a reasonable procedure. In effective medium theory a semiempirical potential is constructed, using a functional form derived from density-functional theory, but with parameters adjusted to reproduce a database of physical quantities and provide a reliable interpolation in other situations.[47,48] The potential includes many-body effects (beyond a pair potential). The surface energies are obtained using a slab geometry and the potential has short range per construction (it includes second nearest-neighbor interactions). All quantities are calculated in real space in a sufficient large unit cell. For ordered phases, finite-size effects is immaterial, but in cases of possible incommensurable reconstructions we have varied the size of the unit cell to verify our results. In the case of random surface phases, ensemble averages have been performed explicitly. In cases where local relaxations are included, each random atomic configuration in the ensemble is relaxed locally before evaluating the energy of the atomic configuration. The average of these energies is the energy of the corresponding random phase.

IV. PSEUDOMORPHIC MONOLAYER SURFACE ALLOYS

We first consider the simplest case where the overlayer grows pseudomorphically on a substrate of A atoms and we neglect the possibility of ordered overlayer structures. Later we consider cases where the deposited metal takes on a different, ordered structure along the surface or where it prefers to migrate to the second or third layer. The case of a pseudomorphic surface phase naturally divides into two subcases, where either pure surface layer phases in the form of large patches with like atoms or surface alloy phases are formed.

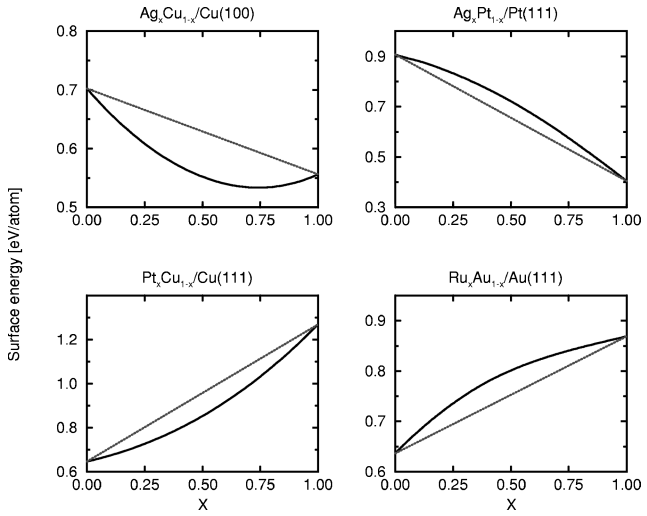

FIG. 2. Examples of surface energy curves belonging to each generic class obtained by LMTO-CPA calculations. For substrate structure and lattice constant the proper bulk values are used. All calculations were performed in the paramagnetic state.

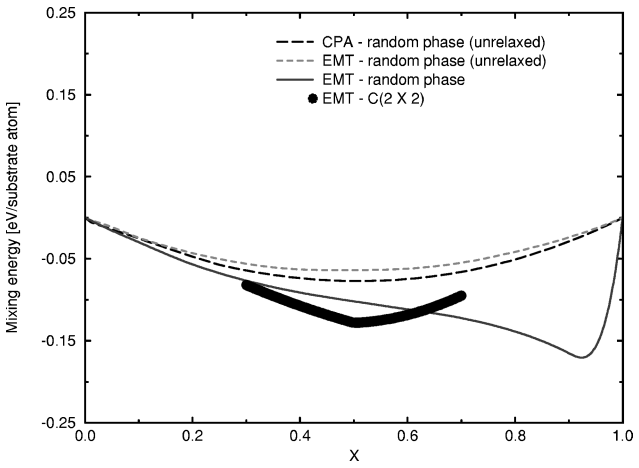

FIG. 3. Surface (mixing) energy of different Ag/Cu surface overlayer phases on a Cu(100) substrate obtained by LMTO-CPA and by EMT. The mixing energy is the difference between the phase-separated state (straight line in Fig. 2) and the surface energy curve.

This is illustrated in Fig. 1(a). In both subcases, the first layer has composition $A_{1-x}B_x$, and the bulk, which is pure A, is assumed infinite. This is therefore the zero concentration limit of the impurity B in metal A.

If we plot the surface energy per substrate atom of the system as a function of the concentration x of the deposited atoms B in the first layer, the surface energy curves are in most cases even simpler than suggested in Fig. 1(b). These surface energy curves fall into four *generic classes*. An example of a binary alloy system belonging to each generic class is shown in Fig. 2.

Consider now the case where metal B is deposited on pure metal A. If the segregation energy is negative, i.e., $de_s/dx<0$, cf. Eq. (5) at $x=0$, as in Fig. 2 (upper row), the deposited material stays in the surface layer. If, on the other hand, the segregation energy is positive as in Fig. 2 (lower row), the deposited material will eventually dissolve into the bulk. As discussed above, the global thermodynamic equilibrium state may not be established immediately for kinetic reasons and a metastable surface state where the deposited material stays in the surface region may exist.

The surface energy curve possesses another important feature, namely its curvature, expressing the B-B excess interactions in the surface layer. By excess interactions we mean interactions beyond that in an ideal solution, where all atomic arrangements (alloyed or dealloyed) are equally stable. A straight line connecting the surface energy of the clean surface ($x=0$) and that of a monolayer of deposited material ($x=1$) represents the ideal solution behavior with no B-B excess interactions, see Fig. 2 (dotted lines). One way to realize a situation with no excess B-B interactions is by having large areas of A and B phases in the surface. The dotted line therefore also represents the surface energy curve for the case of 2D phase separation.

The difference between the straight line and the actual curve is the mixing energy of the random surface solution. When this is negative, corresponding to repulsive B-B excess interactions, as in Fig. 2 (left column), surface alloying, stable or metastable, occurs. If the mixing energy is positive on the other hand, as in Fig. 2 (right column), corresponding to attractive B-B excess interactions, we expect phase separation (island formation) in the surface solid solution.

There are obviously more possibilities if the B-B excess interactions depend on the coverage, but typically, for a given alloy system, the sign of the B-B excess interactions is the same for all concentrations x and the four cases in the figure will encompass the most common cases. It is interesting to note, that in the Ag-Cu(100) system, see Fig. 2, the Ag-Ag excess interaction in the surface is repulsive, whereas it is attractive in the bulk phase, as seen from the bulk heat of mixing.[49] This sign reversal is driven by strain effects in the surface layer, caused by the size mismatch with the Cu substrate in the second layer.

V. ORDERED STRUCTURES AT SURFACES

There are a number of cases where additional phases must be considered. For instance, ordered phases may exist at certain stoichiometric ratios $\{x\}$. If these phases are more stable than the corresponding random state in cases like Fig. 2 (left column) or the phase-separated state in cases like Fig. 2 (right column), phase transitions involving these structures may occur. As an example we consider Ag on Cu(100) in more detail. In Fig. 3, we plot the surface mixing energy, which is the energy difference between the phase-separated (dotted line) and surface alloy phases in Fig. 2. In Fig. 3, we have shown the mixing energy of the unrelaxed random phase (dashed curves) obtained by LMTO-CPA and by EMT. It is seen that the CPA and EMT results are in quite reasonable agreement, and we may therefore use the EMT to consider relaxation effects and the mixing energy of ordered alloy phases. The energy difference between the unrelaxed (dotted curve) and relaxed (solid curve) random phase show that relaxation effects are large in this surface alloy in the Ag-rich end. These large relaxation effects are due to the large size mismatch, Ag atoms having a 13% larger atomic radius than the Cu atoms, that fixes the substrate lattice constant.

We have also included in Fig. 3 the energy of an ordered

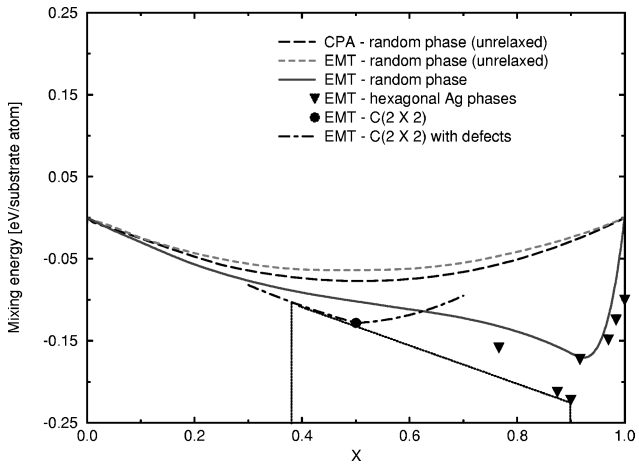

FIG. 4. Surface (mixing) energy of the Ag/Cu surface overlayer on a Cu(100) substrate obtained by LMTO-CPA and by EMT under various conditions. The thin dotted line shows the expected phase transition to hexagonal phases at $T=0$ K.

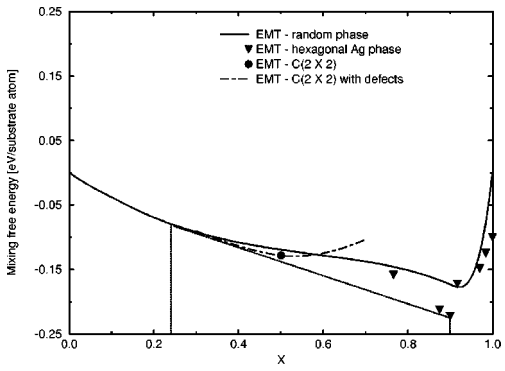

FIG. 5. Surface free energies of mixing of the phases in Fig. 4, but now at $T=300$ K, obtained by adding the mixing entropy term, Eq. (7). The entropy term shifts down the disordered phases by approximately 0.01 eV/atom. This decreases the coverage where the phase transition to hexagonal phases begins, to $x\sim0.24$ (dotted line). We have only included phases that determine the equilibrium.

phase, the $c(2\times2)$ structure (bold dot) at $x=\frac{1}{2}$. At each side of the $c(2\times2)$ point we have calculated the mixing energy of the $c(2\times2)$ structure with defects (dash-dotted curve), i.e., for $x<\frac{1}{2}$ Ag atoms in the $c(2\times2)$ structure are replaced by Cu atoms and vice versa for $x>\frac{1}{2}$. The numerical value of the slope is different on each side of $x=\frac{1}{2}$ on this curve, because the change in mixing energy when exchanging a Ag atom with a Cu atom in the $c(2\times2)$ matrix differs from the change in mixing energy when exchanging a Cu atom with a Ag atom in the $c(2\times2)$ matrix. The curvature gives the defect-defect interaction energy, and this is also different on each side of $x=\frac{1}{2}$. It is seen that the $c(2\times2)$ is more stable than the random phase around $x=\frac{1}{2}$. The reason is that the large Ag atoms repel each other, and a structure with no Ag-Ag nearest neighbors is preferred.

VI. NONPSEUDOMORPHIC CASES

In Fig. 4 we have included yet another overlayer phase. The pseudomorphic surface layers with Ag-rich composition are rather strained, even after local relaxation. This strain is released, if the Ag-rich surface layer reconstructs into a close-packed phase with an Ag-Ag interatomic distance close to that of pure Ag. We have plotted some candidates (triangles) of hexagonal symmetry in Fig. 4. Many competing hexagonal phases exist, but the most stable we have found is the $c(10\times2)$ at $x=0.9$, which is the one observed experimentally.[27] This will be discussed in more detail below.

We now summarize the $T=0$ phase diagram. For very low Ag coverages the random alloy phase is the most stable one. Due to the Ag-Ag repulsion, there will be a short-range correlation between Ag atoms in the surface layer. At $x>0.3$ the underlying $c(2\times2)$ ordering tendency will become more and more prominent. For $0.38<x<0.9$, a phase transition to the $c(10\times2)$ hexagonal phase is expected to occur. The common tangent is shown in Fig. 4 as a thin dotted line.

Since the energies of the different competing phases in Fig. 4 are extremely small, we have to include entropy effects for a complete description even at room temperature. In Fig. 5 we have added the entropy term corresponding to each phase from Eq. (7) at $T=300$ K. At this temperature, the entropy stabilizes the disordered phases [the random and partially ordered $c(2\times2)$ phases] by an amount of the order 0.01–0.02 eV per surface site. The ordered phases [e.g., $c(2\times2)$ and hexagonal] will have vanishing entropy contribution.

When we include entropy effects, the $c(2\times2)$ structure is not stable, and the phase transition towards $c(10\times2)$, as shown by the thin dotted line in Fig. 5, is predicted to begin at $x\sim0.24$ compared to $x\sim0.38$ at $T=0$. It should be noted that the very small calculated energy differences must be handled with caution, and that the purpose is only to illustrate the different effects that may have to be included in a complete description of a surface alloy phase.

VII. ALLOYING AND ORDERING IN THE SECOND LAYER

The cases where the segregation energy is positive, i.e., $de_s/dx>0$, the deposited metal is expected to go into the bulk, dissolving or forming new phases there. However, in many cases, it is found that the deposited metal prefers to be in the second layer, that is to stay at the surface but to be covered by a layer of substrate material. These cases are divided into important subclasses. The first subclass consists of nonmiscible metals where the surface energy of the deposited metal is much larger than the surface energy of the substrate. The Fe/Cu(111) and Co/Cu(111) systems are extreme examples of this behavior and these systems will be discussed in more detail in Sec. VIII.

In the other subclass, which typically consists of miscible metals, the deposited material may alloy and perhaps form ordered structures in the subsurface layers. This is likely to happen, if the deposited element and the substrate may form bulk ordered alloys and one would expect local order corresponding to that in the bulk ordered phase in the substrate-rich concentration region. As an example of this we will discuss Pd on Cu(110) in this section. Another example is Au on Ag(110).[50,51]

According to the bulk phase diagram[52] there is only one

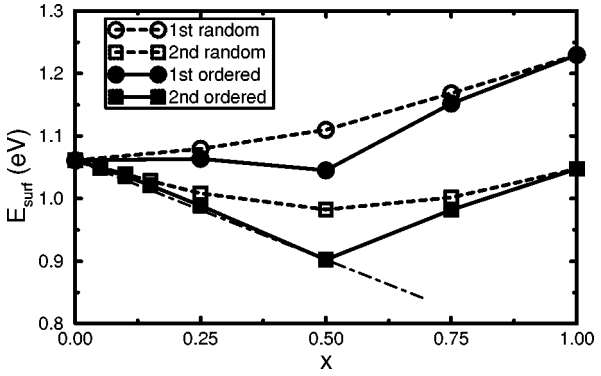

FIG. 6. Calculated surface energies for random and ordered Pd structures in either the first or second layers of a Cu(110) surface, as a function of the fraction x of Pd. The dash-dotted line indicates the phase transition between the pure Cu(110) surface and the ordered (2×1) CuPd alloy in the second layer for Pd coverages $x<0.5$.

ordered phase of CuPd in the Cu-rich region, Cu_3Pd, having the $L1_2$ structure. There are two different types of (110) layers in this ordered phase: pure Cu(110) layers and PdCu(2×1) ordered layers with -Pd-Cu- chains along the [110] direction. Thus, one may expect an energetic preference for the formation of such a type of ordered structure at the Cu(110) surface during deposition of Pd.

In Fig. 6 we show the surface energies of ordered CuPd(2×1) and random alloys in either the first or second layer of an otherwise pure Cu(110). There is complete order for $x=0.5$ and partial order for $x\neq0.5$. To determine the most stable structure for a Pd coverage less than 0.5 ML, it is noted that all other energy points in Fig. 6 lie above the dot-dashed line between the points corresponding to the surface energy of pure Cu(110) and the surface energy of the completely ordered alloy in the second layer (full square at $x=0.5$). This means that if we have $\theta_{Pd}<0.5$, then there will be a phase separation of the system into regions of pure Cu(110) surface and regions (islands) with an ordered (2×1) CuPd alloy in the second layer, covered by a pure Cu layer. The island structure is thus identical to the equilibrium structure of a $Cu_3Pd(110)$ surface which is also terminated by a Cu layer.

VIII. CASES WHERE COMPLETE PHASE SEPARATION OCCURS: Fe/Cu(111) AND Co/Cu(111)

The final case we will consider here is the case where the deposited element forms multilayer structures on the substrate. Again, in this case the common tangent construction may be used as discussed above and in this section we will

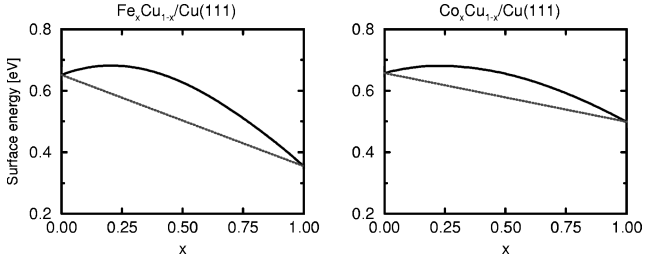

FIG. 7. The surface energies of Cu and Fe on Cu(111) for coverages up to a monolayer.

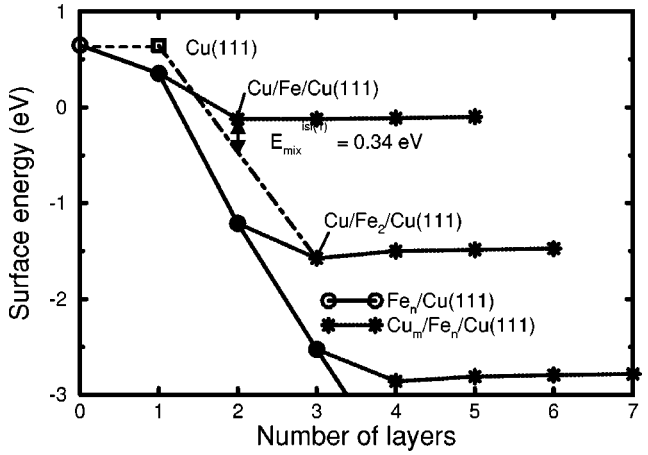

FIG. 8. The surface energies of $Cu_m/Fe_n/Cu(111)$ multilayer structures as functions of the numbers n (open circles) and m (stars). The common-tangent construction is shown by the dashed-dotted curve. See text for further details.

demonstrate such a construction for the case of multilayer Fe and Co structures on Cu(111).

In Fig. 7 we show the surfaces energies of pseudomorphic Fe_xCu_{1-x} and Co_xCu_{1-x} on Cu(111) up to a coverage of one monolayer. In principle these alloy systems belong to the generic class in the lower left corner of Fig. 2, having positive segregation energy at $x=0$ and negative curvature. However, the bulk mixing energy in these alloy systems is so large, that for a certain overlayer coverage the segregation energy becomes negative, and the surface energy drops with increasing coverage. In fact increasing the Fe and Co coverage beyond 1 ML may turn the surface energy arbitrarily negative, the reason being that the bulk phase separation energy is counted as surface energy.

We illustrate this in Figs. 8 and 9 where we show the surface energies of different multilayer structures of Fe and Co on Cu(111), respectively, for coverages up to many monolayers. The solid lines with open circles are the surface energies of X_n/Cu(111) as functions of the number of layers, n. In the following X denotes either Fe or Co. One may see

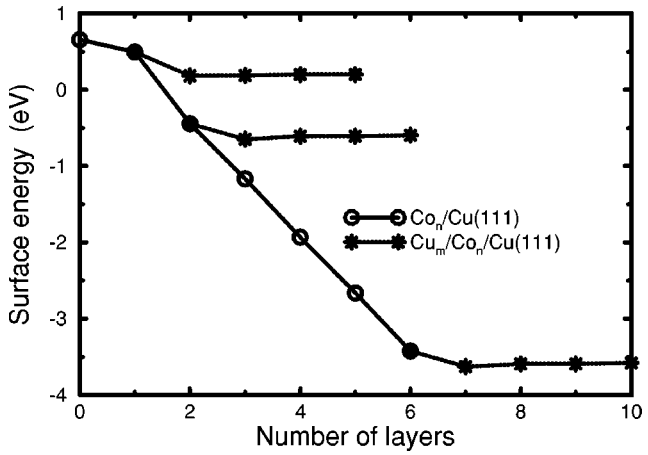

FIG. 9. The surface energies of $Cu_m/Fe_n/Cu(111)$ multilayer structures as functions of the numbers n (open circles) and m (stars). The common-tangent construction is shown by the dashed-dotted curve. See text for further details.

that in both cases the surface energy drops practically linearly with the number of layers. This is a consequence of the fact that there is a strong phase separation in these systems, and thus, in the grand canonical ensemble when there is an infinite source of Fe and Co atoms, the system will constantly undergo phase separation (the slope of the curve at $n \to \infty$ is equal to minus the solution energy of Fe and Co in Cu).

The dotted curves with stars starting from the points corresponding to the X_n/Cu(111) structures are the surface energies of Cu_m/X_n/Cu(111), i.e., X_n/Cu(111) covered by m Cu layers. The following features can be seen to be common for the two systems: (1) the surface energy of the X_n/Cu(111) structure is decreasing when it is covered by Cu atoms; (2) the surface energy does not depend on the number of Cu layers covering a single layer of Fe or Co on Cu(111) while, if the number of Fe or Co layers is greater than one, the Cu/X_n/Cu(111) structure has the lowest surface energy. Therefore, if the number of Fe and Co layers is greater than one, the most stable structure at the surface terminates with a monolayer of Cu.

We may now discuss, whether a single Fe or Co monolayer covered by a monolayer of Cu is stable against separation into other structures. As both these systems exhibit strong phase separation we may safely exclude the possibility of ordered structures (there are no ordered phases in the bulk phase diagrams of the Fe-Cu and Co-Cu systems). Thus, the remaining possibility is a ''phase separation'' of the multi-layer structures, for instance into patches of pure Cu surface and two-layer Fe islands covered by a monolayer of Cu. The corresponding ''mixing island'' energy is

$$E_{\mathrm{mix}}^{\mathrm{isl}(1)} = E_{\mathrm{surf}}^{\mathrm{Cu}/X/\mathrm{Cu}(111)} - \frac{1}{2}\left(E_{\mathrm{surf}}^{\mathrm{Cu}(111)} + E_{\mathrm{surf}}^{\mathrm{Cu}/X_2/\mathrm{Cu}(111)}\right), \quad (10)$$

which is found to be 0.18 eV for Co and 0.34 eV for Fe. From this one may conclude that the monolayer structure is unstable. The common tangent construction corresponding to Eq. (10) is shown by dashed-dotted curves in Fig. 8.

The procedure may be repeated for the two-layer structures [to check against separation into pure Cu(111) and three-layer structure] and iterated until the final most stable multilayer structure is found. It is easy to show, however, that for large n, $E_{\mathrm{mix}}^{\mathrm{isl}(n)} \to 2/(n+1)E_{\mathrm{inter}}^{X-\mathrm{Cu}}$, where $E_{\mathrm{inter}}^{X-\mathrm{Cu}}$ is the Cu-X interface energy. For the (111) surface of Cu-Fe and Cu-Co these energies are approximately 0.1 and 0.2 eV, respectively. Thus, the island mixing energy is positive for any n. This does not mean that such a separation of an initial multilayer structure never ends in real systems. First of all, the island mixing energies become very small with increasing n. Second, in our model we have not included the fact that such an island separation leads to the formation of additional linear and surface defects, which also make the island separation energetically unfavorable. Therefore, as soon as the island mixing energies are sufficiently large and the concentration of the defects accompanying island separation is small, the multilayer structures should be created.

IX. DISCUSSION IN CONNECTION WITH EXPERIMENTAL OBSERVATIONS

In this section we discuss the specific systems that have been used as examples above in the light of available experimental results. First, consider the case of Ag on Cu(100). The findings in the quite complicated phase diagram in Fig. 5 are in good qualitative agreement with recent scanning tunneling microscopy (STM) investigations by Sprunger *et al.*[27] Here, it is found that at low substrate temperatures ($T < 250$ K), Ag deposition results in a $c(10\times2)$ overlayer structure [Fig. 10(a)] on Cu(100). The Ag-$c(10\times2)$ consists of a hexagonal Ag overlayer placed on top of the square substrate lattice [Fig. 10(b)]. This structure is also reported in previous studies employing low-energy electron diffraction,[53] electron energy-loss spectroscopy,[54] angle-resolved ultraviolet photoemission spectroscopy,[55] and photoelectron diffraction.[56]

If Ag is deposited at room temperature and subsequently imaged at lower temperatures (< 200 K), STM results show, see Fig. 10(c), that silver atoms are substitutionally alloyed into Cu(100). In Fig. 10(c) where Ag = 0.4 ML, a small density of Ag-$c(10\times2)$ domains similar to the Ag-$c(10\times2)$ low-temperature structure are observed, but in this case the Ag-$c(10\times2)$ islands are located within the first Cu layer, as revealed from the measured height difference between the Ag islands and the surrounding Cu substrate. Moreover, in the interstitial regions between these hexagonal Ag domains atom-size depressions, attributed to individual Ag atoms being alloyed into the Cu(100) surface, are revealed. This shows the coexistence of two silver phases within the Cu surface: (i) individual Ag atoms alloyed into the surface and (ii) domains of phase-separated $c(10\times2)$ hexagonal Ag islands.

Figure 10 (d) shows an STM image, acquired at 180 K, in which only 0.07 ML of Ag has been deposited at 440 K. At this low Ag coverage only individual Ag atoms, substitutionally arranged within the Cu(100) surface lattice, are depicted, while no hexagonal Ag-$c(10\times2)$ islands are observed. It has been shown that a critical Ag coverage of 0.13 ML exists[27] at which a phase separation occurs into coexisting areas of the alloyed Ag-Cu(100) phase and hexagonal Ag-$c(10\times2)$ islands. The experiments thus agree with the calculated phase diagram, except that the critical coverage for phase separation is 0.13 ML rather than the 0.24 ML found theoretically. The experiments show no sign of an ordered $c(2\times2)$ phase. This is in agreement with the calculated results, but the calculations did not have an accuracy to make any predictions about this. The experiments also show no tendency for Ag to move into the second or deeper layers, in agreement with the results in Fig. 2(a).

From the Ag/Pt(111) surface energy curve in Fig. 2(b) it is seen that the system Ag deposited on Pt(111) is characterized by having a negative heat of segregation and a positive heat of mixing. Thus one would expect that the deposited Ag preferentially segregate to or stay in the surface layer where Ag and Pt should phase separate. The STM studies by Röder *et al.*[28] have shown that if Ag is deposited at room temperature on Pt(111), monatomic height, commensurate Ag islands nucleate and grow at descending step edges. If the surface is annealed to temperatures above 620 K or, alternatively, if the Ag is deposited on Pt(111) at elevated tempera-

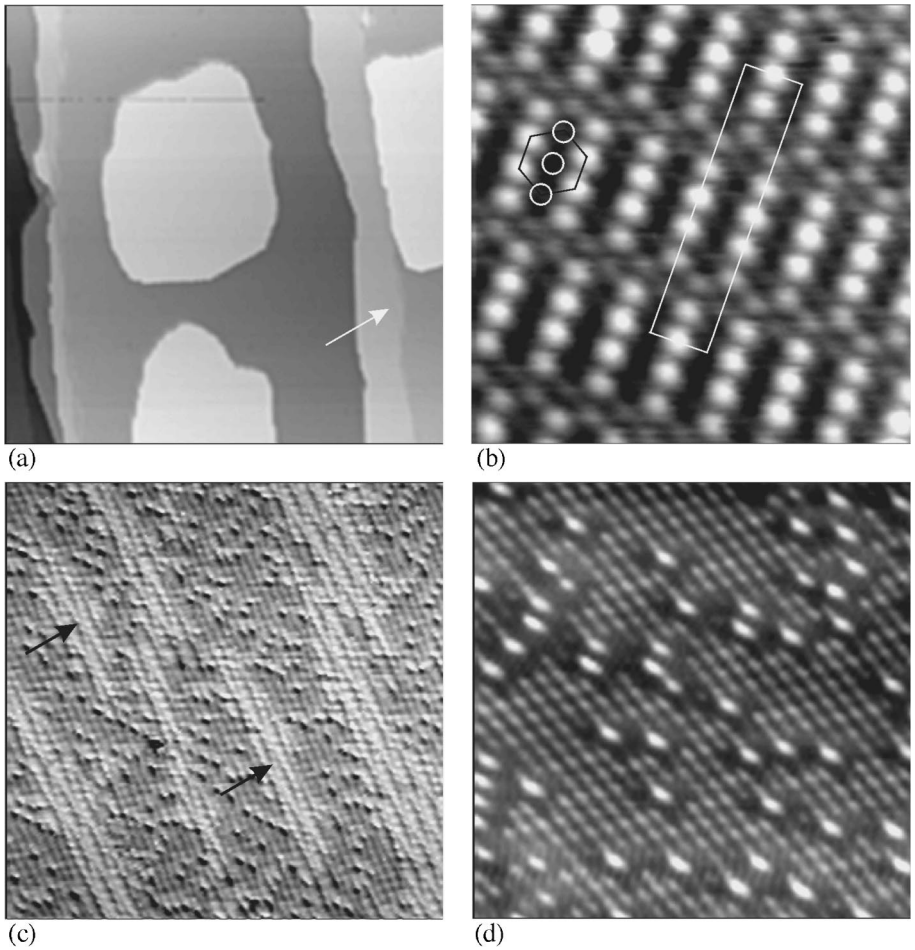

FIG. 10. STM images of Ag deposited on Cu(100): (a) image, revised acquired at 160 K after deposition of 0.4 ML of Ag at 225 K, showing growth of Ag-$c(10\times2)$ overlayer islands on Cu terraces and against step edges (800×800 Å^2; (b) atomically resolved details of the Ag-$c(10\times2)$ superstructure and local pseudohexagonal arrangement (see superimposed grids) (42×44 Å^2); (c) image, acquired at 170 K, of same surface as shown in (a) after annealing to 425 K, showing Ag-$c(10\times2)$ patches within Cu surface (see arrows) surrounded by Ag-Cu alloy (120×120 Å^2); (d) image, acquired at 180 K, of surface deposed with only 0.07 ML of Ag at 440 K showing single Ag atoms (protrusions) pseudomorphically alloyed into Cu(100) surface (56×56 Å^2). From Sprunger *et al.* (Ref. 27).

tures, the Ag dissolves into the Pt surface layer as small Ag islands. The dissolution of Ag into Pt proceeds from the Ag wetted steps, and numerous small protrusions/depressions with a diameter of 10 Å evolve on the Pt(111) terraces and within the Ag islands, respectively. The Ag/Pt dissolution is confirmed by the apparent height difference between these embedded protrusions/depressions and their surroundings. When the Ag-Pt dissolution is fully completed, the most stable cluster sizes correspond to 7, 10, and 12 Ag atoms. The Ag islands are confined to the topmost Pt layer, and increasing the Ag coverage to one monolayer leads to a decreasing density of Pt clusters embedded in Ag until a complete demixing of the two metals is achieved and one is left with a complete monatomic Ag overlayer on top of the nonalloyed Pt(111) substrate. Thus the experimental results fully support the theoretical findings discussed above. However, the stability of various island sizes, shapes, and orientations are finite-size effects. Such information cannot be deduced from the presented calculations, which applies to infinitely large surface phases.

For the Pt/Cu(111) system in Fig. 2(c) a variety of experimental studies have been carried out in recent years, see Refs. 57–61. All studies suggest a layer by layer growth mode of Pt/Cu(111), at least for the first three layers at room temperature. From core-level photoelectron spectroscopy it has been suggested[57] that there exists a sharp interface with almost no evidence for interdiffusion at room temperature. In a later study[58] the same authors conclude that the formation of a Pt/Cu alloy does not occur below a temperature of 580 K. A very recent STM study by Bönicke *et al.*[62] points towards a different behavior for the submonolayer growth of Pt/Cu(111). At room temperature single Pt atoms are found to be alloyed into the Cu(111) surface for low Pt coverages ($\sim$ 0.1 ML). For higher coverages, still below 0.5 ML, the formation of an ordered row-type structure at the step edges, as well as the formation of finger-shaped islands growing out from the steps on the lower terraces are revealed in the STM studies. It is tentatively suggested that the row structure is associated with the formation of an ordered Cu_3Pt surface alloy, but this is at the moment subject to further study.[62] The most recent STM studies thus agrees with Fig. 2 (lower row left).

For the final case in Fig. 2(d), Ru/Au(111), we know of no experiments at present. This is also the least interesting case from a surface science perspective, since the overlayer will dissolve deeper in the crystal and is expected to form (metastable) islands on the surface.

The growth of Pd on Cu(110) discussed in Fig. 6 has also recently been studied using STM by Murray *et al.*[63] At low coverages (Pd$<$0.02 ML), the deposited Pd atoms alloy into the Cu(110) surface to form ordered linear Cu-Pd chains along the $[1\bar{1}0]$ direction. The periodicity of the Pd atoms along the chains, corresponding to two nearest-neighbor distances, is equivalent to that found in a stoichiometric Cu_3Pd bulk alloy. At higher Pd coverages, the linear chains disappear. The Pd atoms become incorporated into subsurface sites, i.e., they become covered, partly with substrate

atoms squeezed out during additional surface alloying, and partly by substrate atoms removed from terraces. Since this mechanism requires more metal atoms to be displaced than Pd atoms deposited, this results in a rough surface morphology with a large number of islands and pits. The islands can be interpreted as regions with an ordered (2×1) PdCu structure in the subsurface layer which is covered with a pure Cu layer, i.e., the island structure is identical to the equilibrium structure predicted by the calculations.

The growth of Co and Fe on Cu(111), the last type of system included here, has been extensively studied. For a review we refer to the paper by Kief and Egelhoff.[64] There are many experimental results showing a bilayer or multilayer epitaxial growth mode for these systems[65–67] and the segregation of Cu to the surface has also been seen at elevated temperatures. The recent STM observations by Pedersen *et al.*[68] show three-layer Co islands. At high temperature there is a tendency to coverage of the Co island by a monolayer of Cu. All of this is in very good agreement with the results of Figs. 7, 8, and 9.

In all cases where experimental results were available, we have found satisfactory agreement with our calculations. In this paper we have proposed a very simple classification scheme for surface alloys, based on four generic classes. In some cases a more complex behavior appeared for various reasons, but in these cases the proposed classification served as a useful starting point.

X. SEGREGATION AND SURFACE MIXING ENERGIES FOR THE TRANSITION METALS

It is clear from the discussion above that a good starting point for an understanding of surface alloy phases are the first and second derivatives of the surface energy with respect to the concentration of one of the two elements. This will immediately indicate which of the four generic classes of Fig. 2 the system belongs to. The first derivative gives the segregation energy through Eq. (5), and the second derivative determines whether the two metals will mix in the surface layer or not: If the curvature is positive there will be mixing, and if it is negative the two metals will not mix in the surface. Knowledge of these two derivatives will not cover the more complex cases discussed above, where there are ordered phases, nonpseudomorphic overlayers or segregation to the second layer, but will still be useful as a guidance for studies of transition metals in and on other transition metals.

Prompted by the above considerations, we have calculated the first and second derivatives in the zero-concentration limit (the initial slope and curvature of the surface energy curves cf. Fig. 2) for all transition- and noble-metal combinations for close-packed surfaces of the equilibrium structure of the host metal, i.e., (111)fcc, (110)bcc, and (1000)hcp. The first derivatives are listed in Table II, while the curvatures are listed in Table III. The values in the tables have been calculated from first principles using the LMTO-CPA method, described in Sec. III. The main limitation of this method is the neglect of lattice relaxations around the impurity. However, since both the segregation energy and surface mixing energies are *differences* in energy for an impurity in the bulk and at the surface, in a large island, or dispersed in the substrate in the first layer, we expect some cancellation of the relaxation energy contributions.

TABLE I. Elastic form parameters derived from EMT.

j	κ_j (eV)	ξ_j (a.u.)
fcc	0.327	1.835
bcc	2.060	3.699
fcc(111)	0.465	1.920
	Curvature relaxation shift	
fcc(111)	−0.800	1.828

To investigate this issue in more detail we have calculated the lattice relaxation energy for impurities at the surface and in the bulk for all host-impurity combinations of the late transition/noble metals (Ni, Cu, Pd, Ag, Pt, Au) using EMT, which describes these metals reasonable well. We define the relaxation energy as the change in total energy, when the impurity and its neighboring atoms are allowed to relax from the perfect crystalline sites defined by the host lattice.

In Fig. 11(a) we show the relaxation energy for impurities inserted into fcc crystal structures versus the host-impurity size mismatch s_A-s_B, s_A, and s_B being the Wigner-Seitz radii of metal A and B, respectively. It is observed, that the relaxation energy is rather well correlated with the size mismatch s_A-s_B. We have also shown a simple anharmonic fit to the data of the form

$$\Delta e_j^{\mathrm{relax}}(s_A-s_B)=-\kappa_j\left[\left(\frac{s_A-s_B}{\xi_j}-1\right)^3+1\right]^2, \qquad (11)$$

which may be used for the common size mismatches for transition metals, -0.8 a.u. $<s_A-s_B<0.8$ a.u., to interpolate the relaxation energy from our data. Subscript j refers to the lattice structure. The two fitting parameters (κ_j,ξ_j) in Eq. (11) are given in Table I for impurities in different lattices.

Papanikolaou *et al.*[69] have recently calculated the relaxation energy around Cu impurities in all the $3d$ and $4d$ transition metals using the full-potential Korringa-Kohn-Rostoker (KKR) Green's-function method. We have included these results in Fig. 11 as open symbols. It is seen that the agreement between their *ab initio* calculations and our EMT results is rather good. The *ab initio* results, which include other transition metals than our EMT calculation, seem to fall on the same curve, supporting the idea that the relaxation energy follows a universal curve, only depending on the lattice structure and size mismatch.

In Fig. 11(b) we have plotted the relaxation energy for an impurity in the fcc(111) surface. It is observed, that the relaxation energy is on average slightly larger at the surface. This is due to the fact that the impurity and surrounding atoms at the surface have more freedom to relax and that the final, locally relaxed structure is less frustrated, than in the bulk. The relaxation correction to the segregation energy is the difference between the relaxation energy for the final and initial situation, see Eq. (5). The result of subtracting the surface and bulk impurity relaxation energy is shown in Fig. 11(c). As anticipated, most of the relaxation energy is can-

TABLE II. Segregation energy (eV/atom) without strain correction for impurity atoms (columns) segregating from a host (rows).

	Ti	V	Cr	Mn	Fe	Co	Ni	Cu	Zr	Nb	Mo	Tc	Ru	Rh	Pd	Ag	Hf	Ta	W	Re	Os	Ir	Pt	Au
Ti		0.12	−0.18	−0.29	−0.33	−0.36	−0.59	−0.80	−0.10	0.48	0.34	0.02	−0.37	−0.55	−0.85	−1.14	0.09	0.53	0.62	0.45	0.17	−0.16	−0.52	−0.85
V	−0.52		0.33	0.51	0.53	0.37	0.03	−0.33	−0.57	0.04	0.55	0.64	0.66	0.46	0.01	−0.38	−0.44	0.21	0.71	1.08	1.17	1.04	0.66	0.21
Cr	−0.65	−0.18		−0.17	−0.59	−0.92	−1.12	−1.32	−1.76	−0.64	−0.02	0.04	−0.36	−1.16	−1.79	−2.01	−1.13	−0.40	0.19	0.52	0.19	−0.50	−1.43	−1.91
Mn	−0.79	−0.10	0.05		−0.14	−0.30	−0.73	−0.92	−1.89	−0.79	−0.22	−0.10	−0.26	−0.49	−0.78	−1.11	−1.47	−0.43	0.04	0.31	0.24	−0.16	−0.55	−0.97
Fe	−0.05	0.48	0.36	−0.02		−0.12	−0.46	−0.85	−1.59	−0.59	0.02	0.11	−0.12	−0.49	−0.78	−1.03	−1.21	−0.28	0.33	0.49	0.33	−0.17	−0.64	−1.02
Co	−0.08	0.30	0.33	0.20	−0.01		−0.17	−0.50	−1.30	−0.08	0.40	0.50	0.32	−0.12	−0.67	−1.16	−0.89	0.02	0.91	0.76	0.81	0.32	−0.32	−1.03
Ni	0.09	0.49	0.37	0.11	0.19	0.16		−0.25	−0.61	0.27	0.85	0.95	0.72	0.28	−0.27	−0.58	−0.45	0.64	1.07	1.28	1.18	0.78	0.14	−0.46
Cu	0.27	0.41	0.14	0.13	0.28	0.27	0.12		−0.08	0.28	0.57	0.55	0.35	0.13	−0.03	−0.28	−0.11	1.00	0.89	0.97	0.76	0.42	0.21	−0.14
Zr	−0.07	−0.01	−0.27	−0.44	−0.59	−0.73	−0.89	−1.09		0.13	0.03	−0.16	−0.36	−0.59	−0.85	−1.08	0.12	0.35	0.33	0.13	−0.13	−0.45	−0.74	−0.96
Nb	−0.34	−0.17	0.01	0.12	0.10	−0.00	−0.22	−0.58	−0.63		0.50	0.67	0.63	0.41	0.04	−0.36	−0.51	0.18	0.64	0.89	0.93	0.73	0.38	−0.08
Mo	−0.23	−0.10	−0.30	−0.60	−0.88	−1.02	−1.16	−1.43	−1.04	−0.13		−0.53	−0.97	−1.28	−1.70	−2.07	−0.39	0.14	0.34	0.22	−0.30	−1.03	−1.52	−1.84
Tc	−0.90	−0.55	−0.30	−0.29	−0.39	−0.51	−0.75	−1.10	−1.33	−0.44	−0.10		0.01	−0.16	−0.56	−1.12	−0.96	−0.32	0.17	0.35	0.26	0.02	−0.34	−0.89
Ru	−0.44	−0.06	0.09	−0.01	−0.25	−0.53	−0.87	−1.35	−0.90	−0.12	0.24	0.27		−0.46	−1.01	−1.74	−0.67	0.08	0.51	0.61	0.39	−0.07	−0.75	−1.52
Rh	0.30	0.49	0.52	0.44	0.26	0.07	−0.17	−0.41	−0.14	0.38	0.64	0.62	0.37		−0.47	−0.92	0.14	0.74	1.01	0.98	0.73	0.31	−0.26	−0.82
Pd	0.86	0.91	0.91	0.77	0.58	0.40	0.22	0.13	0.71	1.27	1.42	1.28	0.93	0.34		−0.30	0.86	1.38	1.64	1.53	1.24	0.77	0.23	−0.14
Ag	0.59	0.64	0.55	0.49	0.41	0.33	0.35	0.15	0.71	0.73	0.79	0.83	0.65	0.46	0.35		0.53	1.38	0.74	0.83	0.58	0.35	0.27	0.07
Hf	−0.16	−0.22	−0.33	−0.46	−0.61	−0.77	−0.94	−1.15	−0.12	−0.04	−0.12	−0.27	−0.50	−0.72	−1.00	−1.28		0.23	0.14	−0.10	−0.36	−0.55	−0.84	−1.08
Ta	−0.55	−0.27	−0.09	0.05	0.06	0.01	−0.23	−0.59	−0.74	−0.20	0.14	0.38	0.42	0.25	−0.10	−0.60	−0.50		0.48	0.81	0.73	0.66	0.38	−0.09
W	−0.29	−0.28	−0.58	−1.03	−1.25	−1.24	−1.28	−1.47	−0.96	−0.38	−0.34	−0.86	−1.50	−1.86	−2.04	−2.52	−0.88	−0.28		−0.32	−1.06	−1.72	−2.06	−2.34
Re	−1.07	−0.64	−0.49	−0.44	−0.49	−0.63	−0.87	−1.30	−1.78	−0.92	−0.42	−0.25	−0.34	−0.58	−0.96	−1.61	−1.51	−0.77	−0.31		−0.02	−0.19	−0.61	−1.21
Os	−0.39	−0.03	0.03	−0.11	−0.33	−0.63	−1.03	−1.52	−1.27	−0.31	0.03	0.00	−0.29	−0.80	−1.46	−2.27	−1.08	−0.19	0.22	0.41		−0.30	−1.25	−2.06
Ir	0.52	0.69	0.74	0.55	0.47	0.22	0.00	−0.18	−0.16	0.50	0.65	0.55	0.27	−0.13	−0.58	−1.02	0.05	0.59	0.82	0.77	0.56		−0.57	−1.12
Pt	0.88	0.98	0.88	0.77	0.63	0.52	0.46	0.32	0.52	1.00	1.12	0.87	0.61	0.25	−0.01	−0.25	0.71	1.23	1.37	1.25	0.99	0.43		−0.32
Au	0.72	0.74	0.70	0.64	0.50	0.45	0.40	0.26	0.78	0.91	0.81	0.62	0.43	0.28	0.15	−0.04	1.25	1.37	1.16	0.93	0.66	0.39	0.21	

TABLE III. Curvature (eV/atom) without strain correction for impurities (columns) segregating from a host (rows).

	Ti	V	Cr	Mn	Fe	Co	Ni	Cu	Zr	Nb	Mo	Tc	Ru	Rh	Pd	Ag	Hf	Ta	W	Re	Os	Ir	Pt	Au
Ti		0.10	1.14	−0.52	−0.03	0.55	0.13	−0.85	0.39	0.08	0.69	1.05	1.14	1.01	0.73	0.60	0.20	−0.24	−0.07	0.51	1.17	1.63	1.69	1.56
V	0.23		0.13	0.51	−0.32	0.06	−0.46	−1.54	1.48	0.40	0.55	1.68	2.15	2.21	1.30	−0.35	1.33	0.21	0.13	1.18	2.21	2.91	2.72	1.81
Cr	1.04	0.21		0.00	−0.26	−0.40	−0.70	−1.36	3.40	1.79	0.86	0.48	0.38	0.36	−0.46	−1.46	3.49	1.84	0.71	0.23	0.56	1.32	1.18	0.44
Mn	2.80	1.44	0.31		−0.07	0.25	−1.74	−0.24	4.82	3.12	1.58	0.91	1.09	1.33	0.93	0.08	4.87	3.38	1.67	0.82	1.11	2.03	2.63	2.73
Fe	1.74	3.58	1.64	−0.94		0.53	−0.84	−1.99	6.75	4.24	2.19	1.14	0.97	0.95	0.46	0.29	6.78	4.50	2.28	1.08	1.02	1.57	1.74	1.87
Co	2.56	1.98	2.60	0.92	−0.04		−0.03	−0.78	8.27	5.64	3.13	1.62	1.12	1.20	1.06	0.59	8.29	6.05	3.37	1.66	1.16	1.54	2.40	2.68
Ni	1.67	1.94	1.47	1.29	1.09	0.00		0.96	10.41	7.29	4.05	1.76	0.86	0.94	1.17	0.99	10.22	7.63	4.36	1.90	0.86	1.07	1.93	2.86
Cu	−0.39	−0.62	1.27	0.34	−1.85	−0.82	0.35		4.38	−0.18	−3.41	−3.68	−1.93	0.02	0.85	1.00	6.14	−1.92	−4.21	−5.38	−3.88	−1.19	0.72	2.19
Zr	0.43	0.08	0.31	0.27	0.21	0.18	0.09	−0.18		0.26	0.41	1.18	1.06	1.05	0.63	0.04	0.03	0.24	0.28	0.80	1.04	1.25	0.94	0.23
Nb	−0.02	0.23	0.63	0.71	0.41	0.00	−0.73	−1.47	0.35		0.45	1.16	1.27	0.64	−0.52	−1.20	0.87	0.03	0.50	1.31	1.74	1.74	0.85	−0.23
Mo	0.72	0.22	0.23	0.00	−0.30	−0.63	−1.03	−1.78	0.87	0.13		−0.21	−0.40	−0.86	−1.73	−2.44	1.00	0.44	−0.00	−0.16	−0.16	−0.28	−0.95	−1.82
Tc	1.79	1.52	0.74	0.55	0.51	0.28	−0.13	−1.47	2.02	1.11	0.26		−0.08	−0.03	−0.56	−1.50	1.93	1.39	0.29	−0.06	0.23	0.50	0.52	−0.10
Ru	2.98	2.02	0.95	0.73	0.72	0.69	0.20	−0.40	4.06	2.26	0.74	−0.08		−0.09	−0.35	−1.11	4.21	2.49	0.70	−0.10	−0.07	0.29	0.52	0.10
Rh	3.81	2.68	1.45	0.72	0.65	0.45	0.30	−0.14	5.91	3.46	1.60	0.32	−0.07		−0.31	−0.79	5.81	3.54	1.29	0.00	−0.31	−0.05	0.22	0.02
Pd	5.07	3.01	1.34	0.50	0.29	0.40	0.42	0.19	8.59	5.28	2.39	0.54	−0.22	−0.19		−0.37	8.20	5.43	2.33	0.12	−0.78	−0.55	−0.03	0.22
Ag	−1.73	−2.85	−2.21	−1.38	−0.15	0.58	0.81	0.33	1.28	−4.30	−4.97	−3.41	−1.15	0.36	0.69		−0.18	−7.70	−6.73	−5.63	−2.90	−0.46	0.50	0.27
Hf	0.05	0.49	0.32	0.15	0.02	−0.02	−0.15	−0.48	0.01	0.79	0.72	0.64	0.64	0.36	−0.11	−0.54		0.45	0.37	0.84	1.11	1.30	1.09	0.44
Ta	−0.39	−0.16	0.26	0.33	−0.12	−0.71	−1.45	−2.24	−0.01	0.03	1.04	1.31	0.93	0.08	−1.20	−1.61	0.03		0.62	1.18	1.37	1.15	0.07	−0.97
W	0.89	0.14	−0.08	−0.27	−0.59	−0.78	−1.14	−1.91	1.08	0.65	0.10	0.07	−0.37	−0.92	−1.76	−2.38	0.97	0.83		−0.03	−0.05	−0.18	−0.85	−1.86
Re	0.84	0.43	−0.11	−0.19	−0.36	−0.54	−1.09	−2.15	1.47	1.12	0.10	−0.13	−0.12	−0.35	−1.12	−2.01	1.67	1.21	0.15		0.07	0.25	0.21	−0.73
Os	2.61	1.63	0.76	0.34	0.22	0.13	−0.35	−1.17	3.47	2.32	0.84	0.08	−0.10	−0.23	−0.98	−2.01	3.79	2.59	0.93	0.03		0.10	−0.16	−0.99
Ir	3.41	2.16	1.24	0.84	0.66	0.55	0.24	−0.48	5.09	3.30	1.44	0.50	0.22	−0.00	−0.51	−1.40	5.29	3.50	1.51	0.18	−0.00		−0.17	−0.76
Pt	4.72	2.78	1.58	0.88	0.76	0.76	0.59	0.16	7.59	4.71	1.98	0.88	0.19	0.25	0.03	−0.41	7.49	5.09	2.18	0.36	−0.20	−0.07		−0.31
Au	0.88	−0.57	−0.61	−0.00	0.76	1.16	1.20	0.65	2.69	−1.48	−2.70	−1.88	−0.31	0.66	0.73	0.22	2.32	−1.72	−3.71	−3.59	−2.05	−0.47	0.22	

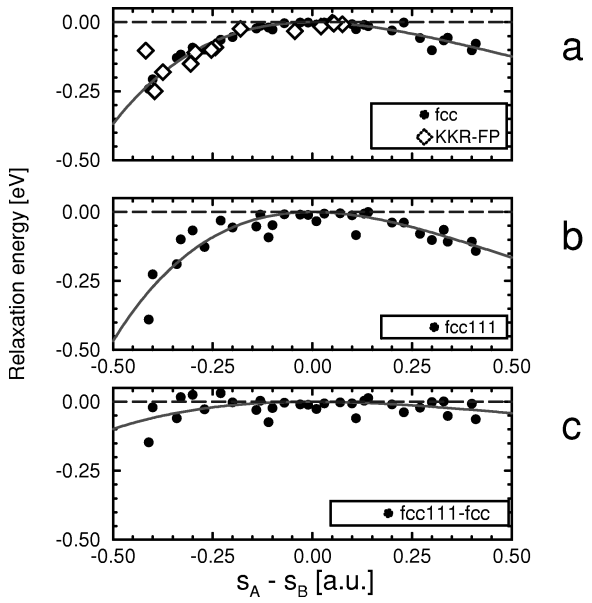

FIG. 11. Relaxation energies for impurities. (a) in bulk fcc, (b) at a fcc(111) surface, and (c) the difference between the energy at an fcc(111) surface and in bulk fcc. The energies were calculated using the effective-medium theory for all binary combinations of (Ni, Cu, Pd, Ag, Pt, Au) shown along with the universal fit by Eq. (11). For comparison we have shown the full potential KKR calculations (Ref. 69) for transition-metal impurities in a Cu crystal.

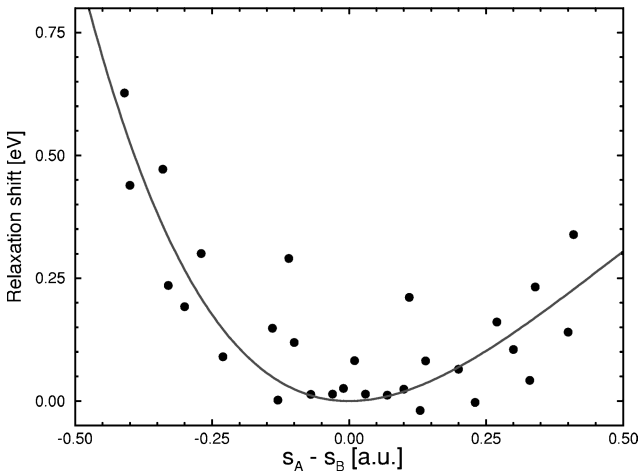

FIG. 12. Estimated shift of the curvature of the surface energy curve $e_s(x)$ caused by local relaxation effects. The curvature shift has been correlated with the size mismatch $s_A - s_B$ between host and impurity metal. All surface alloys in this figure are binary combination of the metals (Ni, Cu, Pd, Ag, Pt, Au). See text for more details.

celled between the surface and the bulk, and for most alloy combinations the relaxation correction to the segregation energy is neglible. A closer inspection reveals, that the sign is very rarely changed by including relaxation corrections. We have therefore only presented the raw, unrelaxed segregation energies in Table II.

We have also investigated the possible influence of relaxation effects on the curvature of the surface energy curve by EMT calculations for the same alloys as above. In Fig. 12 we have plotted directly the change in curvature by including lattice relaxation. On average, relaxation effects make the curvature of the surface energy curve more positive. In most cases, inclusion of lattice relaxation will not change the sign of the curvature. One observes, that significant fluctuations occur around the fitted curve. Therefore we only present unrelaxed curvature data, but we have given the fitting parameters for the fit shown in Fig. 12 in Table I. The relaxation correction can then easily be added, if necessary.

The calculated segregation energies compare very favorably to experiments. Chelikowsky[70] has collected experimental segregation tendencies (the sign of the segregation energy) for 40 combinations of transition metals and compared them to the results of the Miedema rules[71]. The results from Table II agree with experiment in 38 out of the 40 cases. Only for Cr in Fe and Cu in Pt do we predict no segregation, while the experiments suggest segregation. Recent experiments[72] for the Cr/Fe system do, however, indicate that Cr deposited on Fe moves to the second layer, as is the case for Pd on Cu. The segregation energy for Cr to the second layer of pure Fe(110) is -0.08 eV calculated by LMTO-CPA. In the experiment referred to by Chelikowsky, only a Cr surface *region* enrichment was concluded on the basis on Auger electron spectroscopy measurements.[73] Due to the finite escape depth of emitted Auger electrons, only $\sim \frac{1}{4}$ of the recorded signal originated from the surface layer. We point out that the segregation energy for Cu to the second layer of pure Pt(111) is also negative, -0.21 eV calculated by LMTO-CPA. However, surface layer enrichment of Cu in Pt-rich alloys has also been observed by, e.g., low-energy ion scattering,[74] and we expect ordered structures at the surface to be the reason for the apparent disagreement between experiments and our calculations.

The Miedema rules agree with experiment in 38 cases, too, the deviations from experiment being Fe/Zr and Ni/Pt, which are well described by the present results. In terms of the sign of the segregation energy the DFT database of Tables II and III are therefore as good as the Miedema rules. Further, the present database should yield useful absolute numbers, as well as predictions for the surface mixing energy.

XI. SUMMARY

In summary, we suggest that surface alloy phases are conveniently discussed in terms of surface energy diagrams. In the simplest case of pseudomorphic overlayers there are four generic classes characterized by the sign of the first and second derivatives of the surface energy versus surface concentration function. The first derivative is the surface segregation energy and the second is the surface mixing energy determining whether the two components mix in the first layer or form islands.

We have presented *ab initio* results based on the LMTO-CPA method of the two derivatives for all the transition and noble metals to the right of Sc for close-packed surfaces of the host. This provides a data base for surface alloy work as an alternative to the empirical Miedema rules.[71]

Finally, we have considered a number of cases where the simple pseudomorphic overlayer description is insufficient. We have shown that even complicated cases, where there are ordered structures, nonpseudomorphic structures, segregation to the second layer or multilayer formation, may also be treated consistently in the present theoretical framework. In all cases considered the calculated phase diagrams are consistent with available experimental information.

ACKNOWLEDGMENTS

The authors would like to thank Phil Sprunger, Ilva Bönicke, Morten Ø. Pedersen, Erik Lægsgaard, and Ivan Stensgaard for many useful discussions. Financial support from the Danish Research Councils through the *Center for nanotribology* is gratefully acknowledged. Center for Atomic-scale Materials Physics is sponsored by the Danish National Research Foundation.

[1] U. Bardi, Rep. Prog. Phys. **57**, 939 (1994).
[2] J. Wintterlin and R. J. Behm, in *Scanning Tunneling Microscopy I*, 2nd ed., edited by H.-J. Güntherodt and R. Wiesendanger (Springer-Verlag, Berlin, 1994), pp. 39 and 253.
[3] R. Q. Hwang, C. Günther, J. Schröder, S. Günther, E. Kopatzki, and R. J. Behm, J. Vac. Sci. Technol. A **10**, 1970 (1992).
[4] C. Günther, S. Günther, E. Kopatzki, R. Q. Hwang, J. Schróder, J. Vrijmoeth, and R. J. Behm, Ber. Bunsenges. Phys. Chem. **97**, 3 (1993).
[5] D. D. Chambliss, K. E. Johnson, K. Kalki, S. Chiang, and R. J. Wilson, in *Magnetic Ultrathin Films, Multilayers, and Surfaces/ Interfaces and Characterization*, edited by B. T. Jonker *et al.*, MRS Symposia Proceedings No. 313 (Materials Research Society, Pittsburgh, 1993), p. 713.
[6] D. D. Chambliss, R. J. Wilson, and S. Chiang, IBM J. Res. Dev. **39**, 639 (1995).
[7] S. C. Wu, S. H. Lu, Z. Q. Wang, C. K. C. Lok, J. Quinn, Y. S. Li, D. Tian, F. Jona, and P. M. Marcus, Phys. Rev. B **41**, 3353 (1990).
[8] P. W. Murray, I. Steensgaard, E. Lægsgaard, and F. Besenbacher, Phys. Rev. B **52**, R14 404 (1995).
[9] P. W. Murray, I. Steensgaard, E. Lægsgaard, and F. Besenbacher, Surf. Sci. **365**, 591 (1996).
[10] M. Wuttig, Y. Gauthier, and S. Blugel, Phys. Rev. Lett. **70**, 3619 (1993).
[11] Y. Gauthier, M. Poensgen, and M. Wuttig, Surf. Sci. **303**, 36 (1994).
[12] H. P. Noh, T. Hashizume, D. Jeon, Y. Kuk, H. W. Pickering, and T. Sakurai, Phys. Rev. B **50**, 2735 (1994).
[13] R. G. P. van der Kraan and H. van Kempen, Surf. Sci. **338**, 19 (1995).
[14] D. D. Chambliss and S. Chiang, Surf. Sci. **264**, L187 (1992).
[15] D. D. Chambliss, R. J. Wilson, and S. Chiang, J. Vac. Sci. Technol. A **4**, 1993 (1992).
[16] C. Nagl, E. Platzgummer, O. Haller, M. Schmid, and P. Varga, Surf. Sci. **331**, 831 (1995).
[17] S. Rousset, S. Chiang, D. E. Fowler, and D. D. Chambliss, Phys. Rev. Lett. **69**, 3200 (1992).
[18] L. Pleth Nielsen, F. Besenbacher, I. Stensgaard, E. Lægsgaard, C. Engdahl, P. Stoltze, K. W. Jacobsen, and J. K. Nørskov, Phys. Rev. Lett. **71**, 754 (1993).
[19] G. Bozzolo, R. Ibanez-Meier, and J. Ferrante, Phys. Rev. B **51**, 7207 (1995).
[20] J. Tersoff, Phys. Rev. Lett. **74**, 434 (1995).
[21] L. Pleth Nielsen, F. Besenbacher, I. Stensgaard, E. Lægsgaard, C. Engdahl, P. Stoltze, and J. K. Nørskov, Phys. Rev. B **74**, 1159 (1995).
[22] J. Jacobsen, L. Pleth Nielsen, F. Besenbacher, I. Steensgaard, E. Lægsgaard, T. Rasmussen, K. W. Jacobsen, and J. K. Nørskov, Phys. Rev. B **75**, 489 (1995).
[23] J. L. Stevens and R. Q. Hwang, Phys. Rev. Lett. **74**, 2078 (1995).
[24] C. Nagl, M. Pinczolits, M. Schmid, and P. Varga, Phys. Rev. B **52**, 16 796 (1995).
[25] C. Nagl, O. Haller, E. Platzgummer, M. Schmid, and P. Varga, Surf. Sci. **321**, 237 (1994).
[26] D. L. Adams, Appl. Phys. A **62**, 123 (1996).
[27] P. T. Sprunger, E. Lægsgaard, and F. Besenbacher, Phys. Rev. B **54**, 8163 (1996).
[28] H. Röder, R. Schuster, H. Brune, and K. Kern, Phys. Rev. Lett. **71**, 2086 (1993).
[29] H. Brune, H. Röder, C. Boragno, and K. Kern, Phys. Rev. B **49**, 2997 (1994).
[30] C. Günther, J. Vrijmoeth, R. Q. Hwang, and R. J. Behm, Phys. Rev. Lett. **74**, 754 (1995).
[31] C. R. Helms, Surf. Sci. **69**, 689 (1977).
[32] Y. Liu, and P. Wynblatt, Surf. Sci. **290**, 335 (1993).
[33] J. Y. Tsao, Surf. Sci. **262**, 382 (1992).
[34] A. Mosser and A. Jouaiti, Surf. Sci. Lett. **304**, 427 (1994).
[35] A. Senhaji, G. Treglia, B. Legrand, N. T. Barret, C. Guillot, and B. Villete, Surf. Sci. **274**, 297 (1992).
[36] P. W. Atkins, *Physical Chemistry* (Oxford University Press, Oxford, 1990).
[37] J. W. Christian, *Transformations in Metals and Alloys* (Pergamon, New York, 1965).
[38] F. Ducastelle, *Order and Phase Stability in Alloys* (North-Holland, Amsterdam, 1991).
[39] O. K. Andersen, O. Jepsen, and D. Glötzel, in *Highlights of Condensed Matter Theory*, edited by F. Bassani, F. Fumi, and M. P. Tosi (North-Holland, New York, 1985).
[40] O. K. Andersen, Z. Pawlowska, and O. Jepsen, Phys. Rev. B **34**, 5253 (1986).
[41] H. L. Skriver and N. M. Rosengaard, Phys. Rev. B **43**, 9538 (1991).
[42] A. I. Abrikosov, and H. L. Skriver, Phys. Rev. B **47**, 16 532 (1993).
[43] A. V. Ruban, I. A. Abrikosov, D. Ya. Kats, D. Gorelikov, K. W. Jacobsen, and H. L. Skriver, Phys. Rev. B **49**, 11 383 (1994).
[44] J. Perdew and A. Zunger, Phys. Rev. B **23**, 5048 (1981).
[45] S. H. Vosko, L. Wilk, and M. Nusair, Can. J. Phys. **58**, 1200 (1980).
[46] S. L. Cunningham, Phys. Rev. B **10**, 4988 (1974).
[47] K. W. Jacobsen, P. Stoltze, and J. K. Nørskov, Surf. Sci. **366**, 394 (1996).
[48] P. Stoltze, J. Phys. Condens. Matter **6**, 9495 (1994).
[49] R. Hultgren, P. D. Desai, D. T. Hawkins, M. Gleiser, K. K. Kelley, and D. D. Wagman, *Selected Values of the Thermal*

Properties of Binary Alloys (ASG, Metals Park, OH, 1973).
[50] S. Rousset, S. Chiang, D. E. Fowler, and D. D. Chambliss, Phys. Rev. Lett. **69**, 3200 (1992).
[51] C. T. Chan, K. P. Bohnen, and K. M. Ho, Phys. Rev. Lett. **69**, 1672 (1992).
[52] M. Hansen and K. Anderko, *Constitution of Binary Alloys* (McGraw-Hill, New York, 1958).
[53] P. W. Palmberg and T. N. Rhodin, J. Chem. Phys. **49**, 134 (1968).
[54] J. E. Black, D. L. Mills, W. Daum, C. Stuhlmann, and H. Ibach, Surf. Sci. **217**, 529 (1989).
[55] J. G. Tobin, S. W. Robey, and D. A. Shirley, Phys. Rev. B **33**, 2270 (1986).
[56] D. Naumovic, P. Aebi, A. Stuck, P. Schwaller, J. Ostwalder, and L. Schlapbach, Surf. Sci. **307-309**, 483 (1994).
[57] R. Belkhou, N. T. Barrett, C. Guillot, A. Barbier, J. Eugne, B. Carrire, D. Naumovic, and J. Osterwalder, Appl. Surf. Sci. **65/66**, 63 (1993).
[58] R. Belkhou, N. T. Barrett, C. Guillot, M. Fang, A. Barbier, J. Eugne, B. Carrire, D. Naumovic, and J. Osterwalder, Surf. Sci. **297**, 40 (1993).
[59] J. Fusy, J. Menaucourt, M. Alnot, C. Huguet, and J. J. Erhardt, Appl. Surf. Sci. **93**, 211 (1996).
[60] U. Schrder, R. Linke, J.-H. Boo, and K. Wandelt, Surf. Sci. **257/358**, 873 (1996).
[61] Y. G. Shen, D. J. O'Connor, K. Wandelt, and R. J. MacDonald, Surf. Sci. **357/358**, 921 (1996); Phys. Rev. Lett. **71**, 2086 (1993).
[62] I. A. Bönicke, M. Ø. Pedersen, I. Stensgaard, E. Lægsgaard, and F. Besenbacher (unpublished).
[63] P. W. Murray, S. Thorshaug, I. Stensgaard, F. Besenbacher, E. Lægsgaard, A. Ruban, K. W. Jacobsen, G. Kopidakis, and H. L. Skriver, Phys. Rev. B **55**, 1380 (1997).
[64] M. T. Kief and W. F. Egelhoff, Jr., Phys. Rev. B **47**, 10 785 (1993).
[65] J. de la Figuera, J. E. Prieto, C. Ocal, and R. Miranda, Phys. Rev. B **47**, 13 043 (1993).
[66] J. de la Figuera, J. E. Prieto, C. Ocal, and R. Miranda, Surf. Sci. **307-309**, 538 (1994).
[67] J. de la Figuera, J. E. Prieto, G. Kostka, S. Müller, C. Ocal, R. Miranda, and K. Heinz, Surf. Sci. **349**, L139 (1996).
[68] M. Ø. Pedersen, I. A. Bönicke, E. Lægsgaard, I. Stensgaard, A. Ruban, J. K. Nørskov, and F. Besenbacher (unpublished).
[69] N. Papanikolaou, R. Zeller, P. H. Dederichs, and N. Stefanou, Phys. Rev. B **55**, 4157 (1997).
[70] J. R. Chelikowsky, Surf. Sci. **139**, L197 (1984).
[71] A. R. Miedema, P. F. de Châtel, and F. R. de Boer, Physica B & C **100**, 1 (1980).
[72] K. Pfandzelter, T. Igel, and H. Winter, Phys. Rev. B **54**, 4496 (1996).
[73] C. Leygraph, G. Hultquist, S. Ekelund, and J. C. Eriksson, Surf. Sci. **46**, 157 (1974).
[74] H. H. Brongesma, M. J. Sparnaay, and T. M. Buck, Surf. Sci. **71**, 657 (1978).